

The Opportunities and Challenges in the Use of Extra-Terrestrial Acoustics in the Exploration of the Oceans of Icy Planetary Bodies

T. G. Leighton · P. R. White · D. C. Finfer

Received: 6 April 2012 / Accepted: 27 August 2012 / Published online: 13 September 2012
© Springer Science+Business Media B.V. 2012

Abstract Acoustic radiation is the signal of choice for exploring Earth's oceans. Its potential application for the oceans of icy moons requires investigation. However acoustic technology needs to be treated with care for extra-terrestrial purposes. Instruments, calibrations, and predictive codes that have served well on Earth may require fundamental redesign for use on other worlds. However when such an assessment is achieved, acoustic signals open up the possibility of exploring volumes exceeding one million cubic kilometres in a few minutes. This paper begins at tutorial level for novice acousticians, illustrating the principles by which acoustics can be used to monitor the environment at great distances from the source, both by projecting out signals and by using natural signals of opportunity. It then progresses to calculations for a generic icy moon (which resembles, but does not model Europa), proceeding from tutorial calculations of 'flat world' models to calculate the propagation times for pulses to circumpropagate around the entire moon. Given that a single emitted pulse can produce multiple arrivals from different propagation paths, the paper discusses how the structure of the received time history can be used to monitor changes in the temperature profile in the ocean, position of the water/ice layer and the asphericity of the moon during orbit.

Keywords Acoustics · Planetary probes · Oceans · Ray tracing · Circumpropagation

1 Introduction

1.1 Oceans of Icy Moons

The opportunities for the use of acoustics in planetary exploration are significant, as Sect. 1.3 reviews. One of the most promising regions for acoustical exploration would be the vast oceans of icy moons. This paper illustrates why this is so, first by indicating the

T. G. Leighton (✉) · P. R. White · D. C. Finfer
Faculty of Engineering and the Environment, Institute of Sound and Vibration Research,
University of Southampton, Highfield, Southampton SO17 1BJ, UK
e-mail: tgl@soton.ac.uk

advantages that acoustics have brought to ocean exploration on Earth (Sect. 1.2), and then by concentrating on propagation within the ocean of a generic icy moon (Sects. 1.4 onwards).

Massive subsurface oceans are thought to exist inside all of the large icy satellites (Europa, Ganymede, Callisto and Titan) and may have existed (or still exist) inside many others, including Triton and Pluto. Such oceans are generally expected to be 100 km or more deep, beneath ice shells of 10–100 km thickness, and probably are substantially more concentrated in dissolved solutes than are Earth's oceans (Frank et al. 2006; Vance et al. 2007; Sohl et al. 2010; Travis et al. 2012). The presence of such oceans have been inferred from magnetometer data (Zimmer and Khurana 2000), Schumann resonances (Béghin et al. 2010), and their response to tidal forces (Hussmann et al. 2006). Most recently Iess et al. (2012) inferred the presence of a probable layer of water, perhaps 200 km thick, encircling Titan beneath a surface ice shell that is perhaps up to 100 km thick. This was achieved by monitoring the variations in speed of the Cassini probe as it orbited the planet, as determined from the slight Doppler shift in the radio signals Cassini transmitted back to Earth (Rappaport et al. 2008). Changes in Cassini's speed were attributed to changes in Titan's gravitational field as it orbits Saturn. The extent to which the gravitational field is perturbed depends on the deformation of Titan during its marginally elliptical 16-day orbit, which in turn depends on Titan's inner structure, and hence allowed the inference of the existence of a large subsurface ocean.

Although Titan is undoubtedly fascinating, being for example the only moon in the Solar System with a thick atmosphere and surface lakes, its ocean floor is probably cold and icy. Europa in contrast is widely believed to have seabed vents which emit warm water that is rich in chemicals known to be important for the generation of life (Gaidos et al. 1999; Marion et al. 2003; Lipps and Rieboldt 2005). On Earth, seafloor hydrothermal vents support life that is not dependent on solar energy. Europa is therefore a likely candidate to receive exploratory probes in coming decades. This tutorial paper will restrict its illustrative ocean acoustical calculations to examples in the liquid water regions of a generic model moon that resembles Europa (but does not model it, because inclusion of the complexity and possible parameter ranges that represent current knowledge about Europa would detract from the clarity of the pedagogical acoustical arguments).

1.2 Acoustical Exploration of Earth's Oceans

In the twentieth century the concept of 'exploration' became more one of investigating volumes, not areas. The oceans occupy around 72 % of the surface area of the Earth, and around the same proportion of the volume of our planet that contains macroscopic life.¹ Much of this remains unexplored, more people having set foot on Earth's Moon than having visited the deepest ocean regions. Much of the ocean is devoid of significant light or oxygen, yet it is occupied by ~250,000 species (Mason 2003), including intelligent air-breathing mammals that spend hours at a time at depths as great as ~2 km.

Exploration and measurement of the oceans is rarely done by manned vehicles. The slow vehicle speeds mean that the volumes explored via local sampling by unmanned vehicles or remote instrumentation, cannot compare to the volumes which have been explored using acoustics. Sound pulses are the radiation of choice for covering Earth's vast oceanic volumes,

¹ This calculation is based on an assumption that the volume of our world that contains macroscopic life encompasses the oceans, plus a blanket of atmosphere around 1 km thick, overlying a solid surface occupied to the depth of a few tens of metres, a total 'biovolume' of approximately $1.3 \times 10^9 \text{ km}^3$.

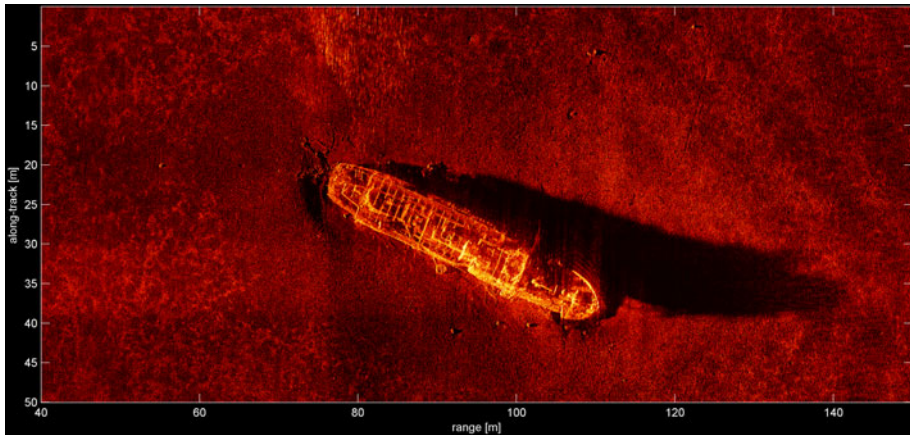


Fig. 1 Sonar image taken by MUSCLE AUV (autonomous underwater vehicle) equipped with dual sided 300 kHz synthetic aperture sonar. The data were collected during the ARISE'11 sea trial in the Ligurian coastal waters. The image shows the wreck off the coast of Riomaggiore of the passenger vessel *Equa*, which was built in 1930, sank in 1944, depth 34–40 m, latitude 44°3.667'N, longitude 9°45.050'E. (Image provided by NATO Undersea Research Centre)

as they travel at around 1.5 km s^{-1} with attenuations so low that they can propagate thousands of times further than an electromagnetic wave of the same frequency before falling to, say, 1 % of their initial amplitudes (Leighton 1994). Even after decades of research sponsored by Government, military and industries throughout the world, acoustics still has untapped potential. This is illustrated by the fact that the echolocation capabilities of dolphins far exceed that of the best man-made sonar even though, on paper, the dolphin would appear to have inferior 'hardware' in terms of power, bandwidth etc. (Au and Martin 2012). Currently, human technology has exploited acoustics in methodologies as diverse as imaging (Fig. 1), Doppler, and the quantification and classification of targets (e.g. biomass, mines etc.). Acoustic waves can readily generate nonlinear effects, for example allowing clutter in images to be made invisible (Leighton et al. 2010, 2011). Measurement of the temperature profile in the ocean was critical to the use of sonar and, more recently, understanding the significance of the oceans to weather and climate. In the past this was measured by the arduous and expensive operation of having a research ship tow an array several km long of thermocouples for weeks or months. This meant that making a snapshot of this seasonal variable was impossible over the scales of an ocean basin. In the 1990s acoustic thermometry was developed whereby a sound pulse could travel half way around the world in about 3 h, and its form on receipt at listening stations around the world could be used to compute 3D temperature maps of the ocean (Worcester et al. 1999; Dushaw et al. 2009). With our visual acuity and eminent history of exploring space through the electromagnetic spectrum, engineers and scientists tend to consider electromagnetic sensing pre-eminent. However in the oceans its use is dwarfed by the power of acoustics.

In addition to the active acoustics demonstrated in Fig. 1, passive acoustics are used in exploration of Earth's oceans. There, natural sources of sound are rife (fauna, ice, seismic activity, weather, waves etc.), and the detection of these emissions can be interpreted to gain information about the source itself and about the propagation path from source to receiver. Passive acoustic systems generally have lower power consumption than active ones, and indeed self-powering sensors (harvesting energy from local currents) will

probably be deployed on Earth's seabed in the next few years e.g. for monitoring methane seeps from the seabed (Sauter et al. 2006; Leifer and Tang 2007; Cook and Masek 2009; Leighton and White 2012). Furthermore they are rugged, relatively inexpensive, and require low bandwidth for the archiving and/or re-transmission of data (compared to, say, video). These advantages are attractive for planetary exploration.

1.3 Sound in Space

Despite the wealth of images from planetary exploration, we have never actually heard the sound of another world (Muir 2007; Leighton and Petculescu 2009). Such sound carries complementary information to imaging, especially given that the available 'field of view' for a microphone array often consists of the above-ground half-space, or the full 4π solid angle underwater; directional information can be obtained from an array of multiple sensors. Thunder, ice, subsea vents, rockslides, dust devils and cryovolcanos are just some of the likely sources of sound.

Despite the attractive features listed at the end of the preceding section, for much of the history of extraterrestrial exploration, the importance of acoustics has perhaps been underrated (Leighton 2007; Leighton and Petculescu 2008). Of the few probes that carried microphones, the most successful acoustic measurements were made by the European Space Agency's 2005 *Huygens* probe to Titan. Although this probe was spectacularly successful in measuring the atmospheric sound speed and estimating the range to the ground using an acoustic signal that the probe itself emitted (Fulchignoni et al. 2005; Zarnecki et al. 2005; Towner et al. 2006; Hagermann et al. 2007) we still have no measurements of sounds generated by alien worlds themselves. Although microphones have been built for Mars (Delory et al. 1998), the *Mars Polar Lander* was lost during descent on 3 December 1999, and the *Phoenix* probe microphone was not activated (because the Mars Descent Imager system to which it belonged was deactivated for fear of tripping a critical landing system). Instead of measuring acoustic signals that had propagated to the microphone from a distance, aerodynamic pressure fluctuations on the microphone masked the soundscape on Venus and Titan missions. These aerodynamic fluctuations were caused by wind on the surface of Venus in the case of the 1982 Russian *Venera* 13 and 14 probes (Ksanfomality et al. 1983a, b) and turbulence during the parachute descent in the case of *Huygens*. They do not represent sound, but merely local pressure fluctuations that do not propagate to distance.²

Given the lack of such data from these earlier missions, some early enthusiasts for acoustics in the space community are now sceptical as to whether it will ever have useful role. However basing such an assessment on past performance presupposes that the sensor systems have been optimized for the environment in question. Cutting edge acoustical capability goes far beyond what is commercially available, yet even the latter holds potential solutions to problems that limited past missions. For example, the aerodynamic pressure fluctuations that prevented measurement of the soundscape by *Venera* and *Huygens* might have been mitigated by the deployment of appropriate microphone windshields (extraterrestrial versions of those used by journalists to report from stormy locations) or the use of two or more synchronized microphones to separate the real acoustical signals from aerodynamic pressure fluctuations (Wang and Crocker 1974; Shepard and La Fontaine 1986; Sebald and Van Veen 1996). At the cutting edge, appropriate models of the

² Just as waving one's hand underwater (without breaking the surface) in the bath next to a submerged ear creates a loud signal which does not propagate to elsewhere in the bath, and so is not an acoustic signal. In contrast, breaking the surface traps bubbles, which do general acoustic signals to distance.

generation and propagation of sounds are today being inverted to allow the use of passive acoustics listening devices to estimate key environmental parameters (such as rainfall at sea, tornado detection, animal location, icecap erosion, crack formation in aircraft wings, erosion in hydroelectric turbines, and the progress of medical treatment, in addition to the established techniques for seismic and global test ban monitoring (Medwin 2005; Leighton et al. 1998, 2003, 2008a; Stafford et al. 1998; White et al. 2006; Bass and Yan 1994; Hadcock et al. 1991; Brecht and Ginzkey 2000). Given the vast expense involved in sending an acoustic sensor to another world, it is important that that sensor be properly designed for the alien environment, and that the data it detects be sufficiently free of artefacts so that it can be interpreted correctly. Detailed modelling of acoustic characteristics of alien worlds is therefore vital to the design of instrumentation, the planning of the acoustical components of the missions, and the correct interpretation of the data. If the astronaut from the future is walking down a Martian hillside, looking downwards, can we design microphones to warn him of the fall of a rock dislodged behind him? Since acoustic absorption is so great in the atmosphere of Mars (Petculescu and Lueptow 2007), then perhaps a space suit for that planet would need its ‘ears’ on its boots (as opposed to helmet) so that they can pick up ground-transmitted signals. The temptation to treat acoustics as a known science with off-the-shelf components that can be adapted for planetary probes should be avoided. For example, state-of-the-art acoustical engineering shows that a long-standing design of an acoustical sensor proposed for Venus, and now under consideration for use in the gas giants, would generate misinformation unless a very careful choice of materials is made (Jiang et al. 2011). As another example, fluid loading effects (usually ignored on Earth) could generate discrepancies of tens of percent in the natural frequencies and hence calibrations of sound sources and sensors that are designed and calibrated on Earth and then sent to Venus (Leighton 2009). Underestimation of the acoustical problems of a mission will lead to wasted effort. However rigorous acoustics, followed through from fundamentals to final application, allow appropriate acoustical protection of components during launch (Leighton et al. 2012), prediction of the sounds of Titan’s lakes (which in turn allows appropriate instruments to be designed to hear these sounds—Leighton et al. 2005; Ainslie and Leighton 2009), and assessment of ways in which acoustics can be used to explore icy moons.

1.4 Generic Icy Moon Model

Of the many environments where acoustics could provide a useful tool, the oceans of icy moons are particularly interesting, because they are inaccessible to probes, and merit sampling over vast distances.

This paper sets up a generic model ocean in an icy moon and proceeds through a tutorial to illustrate key acoustical principles by undertaking ‘flat world’ propagation calculations (Sect. 3). The advantage of such calculations is that they can be done analytically and explain all the principles behind the numerical calculations required when the curvature of the moon is taken into account (Sect. 4). Discussion of the errors inherent in using flat world model (Sect. 4.1) is used to progress from the tutorial stage to express the results of the numerical model for the curved world (Sect. 4.2 onwards).

The generic icy moon is chosen to resemble Europa, but not mimic it because the complexity and uncertainty associated with key parameters in Europa would muddle the tutorial element. Several notable acoustical investigations have in the past featured Europa. Kovach and Chyba (2001), Makris (2001), Makris et al. (2001) and Lee et al. (2003) produced pioneering studies which modelled acoustic propagation in the ice and the sub-

ice ocean of Europa. They opened the way for assessing Europa's ice and ocean using acoustical signals of opportunity, generated by natural processes in the ice, ocean or below the seabed (Crawford and Stevenson 1988; Schenk and McKinnon 1989; Hoppa et al. 2000; Greenberg 2002; Lee et al. 2003, 2005; Nimmo and Schenk 2006; Panning et al. 2006). However propagation over distances characteristic of the depths of Europa's oceans (which exceed the maximum depths of Earth's oceans by an order of magnitude), or propagation over the length-scales that typify the separation of major ice cracking events that could generate sources of opportunity for acoustic measurements, require use of a model which departs from those developed for terrestrial use (Leighton et al. 2008b).

Perhaps the most important feature in the use of acoustics to explore the deep ocean has been our ability to model the way sound rays refract in response to variations in water temperature and hydrostatic pressure (and to a lesser extent, other features, notably salinity). This will be introduced in Sect. 2. In Earth's deep ocean water, hydrostatic pressure is almost always the dominant term, because at depths of 1 km or more from the air/sea boundary the temperature usually does not change significantly, whereas the hydrostatic pressure increases inexorably by roughly an additional 1 bar (10^5 Pa) with every 10 m extra depth. From the simplest student algorithm to the most sophisticated 3D code for ocean acoustic propagation on Earth, the hydrostatic pressure (P_h) is expressed as $P_h = \rho_w g z$, where ρ_w is the liquid density, g is the acceleration due to gravity (taken in Earth ocean calculations to be constant at the value it had at the air/sea interface), and z is the depth below the air/sea interface on Earth. However characterising the hydrostatic pressure as $P_h = \rho_w g z$ is an approximation derived from the exact expression $\nabla P_h = \rho_w g$. The relationship $P_h = \rho_w g z$ only arises when $\nabla P_h = \rho_w g$ is integrated and two assumptions are made: that g does not vary with z , and that the Earth is flat, allowing the equivalence $\nabla \equiv \partial/\partial z$. These approximations can lead to very large errors when applied to bodies of similar dimensions to Europa's structure (Leighton et al. 2008b). This is because the substantial depth of the ocean (~ 100 km) leads to significant variation of the gravitational acceleration through the water column, and the change in radial distance from the planet's core is so great, and so close to the core, that $\nabla \neq \partial/\partial z$. Consequently, the established codes for ocean acoustic propagation on Earth cannot be applied to the oceans of icy moons without caution.

A more obvious limitation of the 'flat world' model is when the acoustic propagation occurs to ranges that are an appreciable fraction of the planet's radius. Under such circumstances it is not just details of the ray path which deviate from the flat world model, but so too do the locations of the seabed and upper ocean surface. An extreme case of this is circumpropagation, the propagation of sound through the liquid ocean, right around the planet under the ice and back to the source. In such propagation, three-dimensional refocusing might occur at the source and at the point on the planet opposite the source (because, in simple terms, the spreading losses that occur during propagation over one hemisphere are, for ideally spherical conditions, reversed on the broad scale as the waves propagate over the other hemisphere). Because of these key end-points, circumpropagation provides scenarios which can be studied using simple calculations to assess sensitivities in a transparent manner.

Section 2 sets up the generic icy moon ocean model that is used throughout this paper. It is used in Sect. 3 (for 'flat world' modelling) and in Sect. 4 (in a circumpropagation model) to demonstrate how the environmental parameters can affect the propagation. A long term goal of such studies is the demonstration of how the inversion of measured acoustic propagation could be used to estimate or monitor the values of those parameters. This is specifically demonstrated in Sect. 3 by considering how a sound pulse from a probe on the

seabed can be used to test models of the ocean temperature for hundreds of kilometres around the probe in a few minutes. These flat world calculations are replaced in Sect. 4 by propagation predictions for a simple model which assumes uniform temperature throughout the ocean (not an unreasonable first order model, given the presence of convection; Grasset et al. 2000), for the case of propagation of sound around the planet back to the source (circumpropagation). Whilst the assumed conditions only pertain to the generic icy moon ocean, and are not specific predictions for any given world, they serve to demonstrate the sensitivity of the arrival times to the ocean temperature, and to the positions of the seabed and the base of the ice shell. In particular it shows how monotonic change in a particular environmental parameter (such as moon shape or ocean temperature) during orbits around a planet and sun, can result in qualitative changes to the ray paths and hence threshold discontinuities in acoustic travel times. As a result, the effect on observables such as the arrival times can be very much greater than a simple linear scaling would predict.

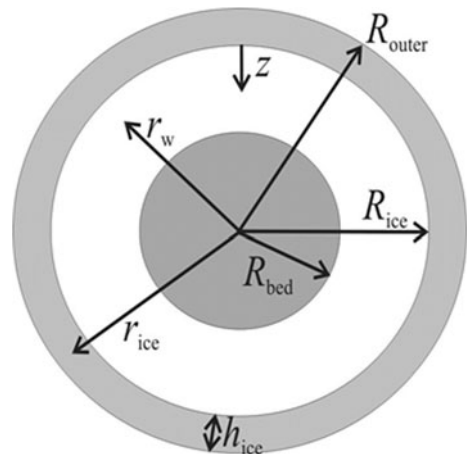
2 Method

2.1 Refraction in the Generic Icy Moon Ocean

The calculations will be done for an idealised spherical layered moon. The general features and scales resemble Europa (Nimmo et al. 2007) but the parameter values chosen, and their depth dependence (or lack of it) are not meant to describe Europa, but to provide a simple tractable model world in which the baseline illustrations of this paper can be undertaken. In this way the potential of acoustics can be illustrated for a non-acoustician readership, without being complicated by a mass of detail as the possible effects of the allowable ranges of structure, composition, time-dependencies etc. currently attributed to Europa (VanHoolst et al. 2008).

The model spherical world has an outer radius R_{outer} , where a layer of ice (of thickness h_{ice}) overlies an ocean (of thickness $R_{ice} - R_{bed}$) that is assumed (for the moment) to have a uniform temperature. The geometry is shown in Fig. 2, and the parameter values for this ocean, are as follows. The outer radius of the world (the distance from the centre to the top of the ice layer) is $R_{outer} = 1,560,800$ m. The radius at which the seabed occurs is is

Fig. 2 Cross-section of the model moon labelling key fixed ($R_{bed}, R_{ice}, R_{outer}$) and variable (r_w, r_{ice}) radii



$R_{bed} = 1,440,800$ m. Let ρ_w and ρ_{ice} be the densities of the water and ice respectively in this world (neglecting any variation of these with depth, and any complexities in the chemical composition; Spohn and Schubert 2003; Frank et al. 2006) and let ρ_E be the spatially-averaged density of the seabed, mantle and core: these are assumed for convenience to take constant values of $\rho_w = 1,000 \text{ kg m}^{-3}$, $\rho_{ice} = 920 \text{ kg m}^{-3}$, with $\rho_E = 3,550 \text{ kg m}^{-3}$. The first set of calculations assume that the water/ice interface occurs at a radius of $R_{ice} = 1,540,800$ m, such that the water column is 100 km deep (i.e. $R_{ice} - R_{bed}$ is constant at 100 km) and the ice layer thickness ($h_{ice} = R_{outer} - R_{ice}$) is fixed at 20 km deep (although in Sect. 4 the position of the ice/water interface is allowed to change). Given a moon of mass M , these initial values give the generic model moon a normalized mean moment of inertia (I_{nm}) of:

$$I_{nm} = \frac{8\pi (\rho_E R_{bed}^5 + \rho_w (R_{ice}^5 - R_{bed}^5) + \rho_{ice} (R_{outer}^5 - R_{ice}^5))}{15 MR_{outer}^2} \approx 0.36 \tag{1}$$

an indication of the extent to which this simple generic model moon would differ from a simplified model of Europa (for which Anderson et al. 1998 estimated an I_{nm} of 0.346 ± 0.005).

Because the sound speed increases with increasing ocean depth, if ray tracing were to be appropriate for sounds emitted in the ocean, a simple Huygens’ wavelet construction shows that the propagation would be upwardly refracting (Fig. 3). Such long range propagation under Earth’s Arctic has been studied with considerable success (Mikhalevsky and Gavrilov 2001).

On Earth, the radius of the planet is sufficiently large, and the depth of the ocean is sufficiently shallow, that rectilinear (‘flat world’) calculations assuming constant gravitational acceleration are accurate for the vast majority of predictions. A ‘flat world’ approach is outlined in Sect. 3. However on the generic icy moon of the dimensions used here, ‘flat world’ techniques may be insufficiently accurate over the path of such a ray, and therefore methods incorporating curvature and variable gravitational acceleration have been developed (Sect. 4).

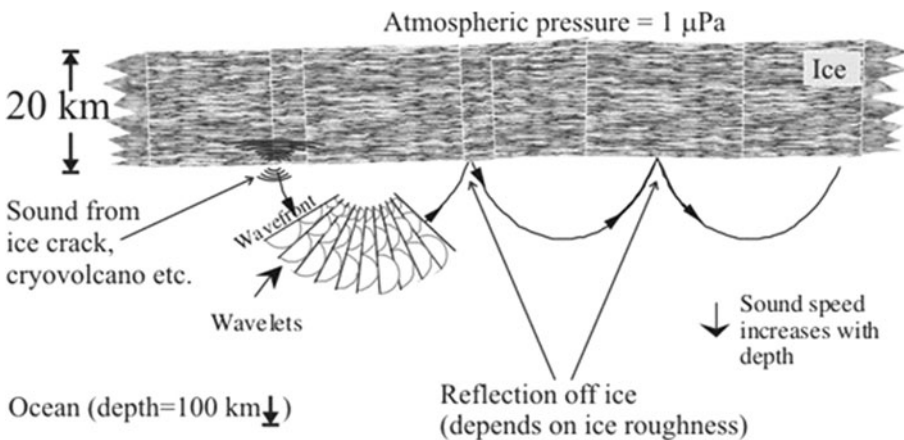


Fig. 3 Schematic of the refraction and reflection of sound. A source of sound at the base of the ice field emits into both water and ice. The ocean is upwardly refracting. This can be seen from the Huygens’ wavelet construction. As a result, the sound returns to the ice from where it is reflected (with fidelity depending on the smoothness of the ice), to continue along the ocean through subsequent refraction and reflections

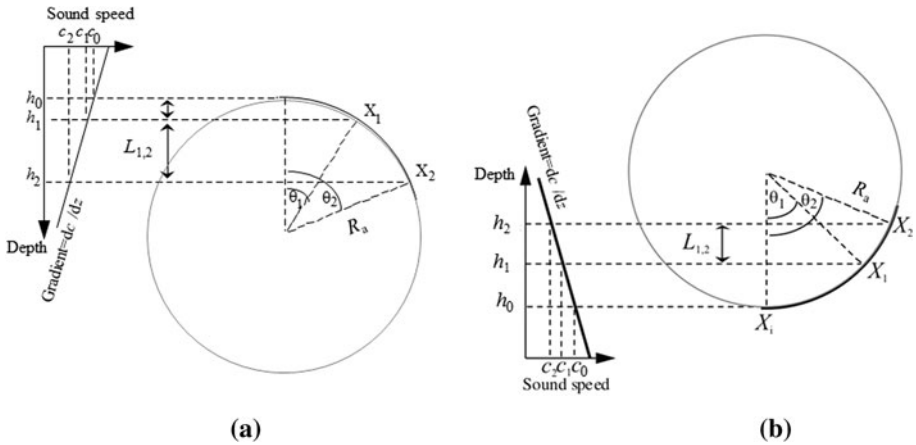


Fig. 4 Ray paths in a region of ocean where the sound speed **a** decreases and **b** increases linearly with depth. There are no variations of sound speed in the horizontal direction

2.2 Oceanic Ray Tracing

Consider Fig. 4, where the sound speed (a) decreases and (b) increases linearly with increasing depth (z). Both scenarios are common in Earth’s oceans, depending on the temperature variation with depth, and the formulation below is equally applicable. The sound speed changes linearly from c_1 (at depth h_1) to c_2 (at depth h_2). The sound ray passes through points X_1 and X_2 at depths h_1 and h_2 . Join the two points by a circle: the circle is horizontal at a depth h_0 , where the sound speed is c_0 . From the geometry of Fig. 4, if the raypath followed the arc of a circle, then that circle must have a radius R_a where the distance $L_{1,2}$ is equal to:

$$|h_2 - h_1| = |R_a \cos \theta_1 - R_a \cos \theta_2| \tag{2}$$

Since there is a linear variation in sound speed,

$$|h_2 - h_1| = \left| \frac{(c_2 - c_1)}{dc/dz} \right| \tag{3}$$

If the ray is acoustic, then it must satisfy Snell’s law, such that

$$c_1 = c_0 \cos \theta_1 \quad \text{and} \quad c_2 = c_0 \cos \theta_2, \tag{4}$$

(since $\cos \theta_0 = 1$). Substitution of Eq. (4) into Eq. (3) implies that

$$|h_2 - h_1| = \left| \frac{(\cos \theta_2 - \cos \theta_1)c_0}{dc/dz} \right|. \tag{5}$$

Eliminating $|h_2 - h_1|$ and $\cos \theta_1$ and $\cos \theta_2$ from Eqs. (2) and (5) implies that, when the sound speed varies linearly with depth only, this acoustic ray follows the arc of a circle of radius

$$R_a = \left| \frac{c_0}{dc/dz} \right|. \tag{6}$$

Put another way, the raypaths in Fig. 4 follow arcs of circle because R_d is constant if dc/dz is constant.

Equation (6) can be utilised in simple illustrative examples if it is assumed that the sound speed profile varies approximately linearly with depth throughout the ocean. For such examples, the sound speed profile in the ocean (the plot of the sound speed as a function of the depth from the bottom to the top of the water column) can have constant gradient throughout the water column, or be divided into sections, each with its own gradient. Simple examples are given in Sect. 3.

The same principles can be used to calculate ray propagation in less simple profiles, for example by dividing the ocean into layers in which the sound speed profile has constant gradient (White 2004). The approach adopted in section 4 is based on expressing the ray paths as solutions to a pair of ordinary differential equations (Jensen et al. 2000). These equations can be solved using standard numerical routines. Whilst variations of sound speed in the lateral direction are possible, these are not incorporated into this modelling.

3 Results of Analytical ‘Flat World’ Calculations

The speed of sound (c) in the Earth’s oceans is often characterized using one of a number of similar empirical equations resembling:

$$\begin{aligned} c/c_{\text{ref}} \approx & 1449.2 + 4.6T/T_{\text{ref}} - 0.055(T/T_{\text{ref}})^2 + 0.00029(T/T_{\text{ref}})^3 \\ & + (1.34 - 0.010T/T_{\text{ref}})(S/S_{\text{ref}} - 35) + \alpha P_{\text{h}}/P_{\text{ref}} \end{aligned} \quad (7)$$

where c is a function of temperature (T), salinity (S) and hydrostatic pressure P_{h} (which excludes atmospheric pressure so that it is zero at the ocean surface of Earth). The appropriate reference values are $c_{\text{ref}} = 1 \text{ m s}^{-1}$, $T_{\text{ref}} = 1 \text{ }^{\circ}\text{C}$, $S_{\text{ref}} = 1 \text{ g kg}^{-1}$ (grams of dissolved salt per kilogram of sea water), and $P_{\text{ref}} = 1 \text{ Pa}$. There are many choices available for empirical expressions such as (7) to describe the effect of temperature, salinity and hydrostatic pressure on the sound speed in the ocean (Urlick 1983; Medwin and Clay 1998; Chen and Millero 1977; Fofonoff and Millard 1983). Equation (7) is the form selected for tutorial acoustic propagation modelling in icy moons of the dimensions used in this paper (Leighton 2012). It is important to note that use of this equation in this paper is to provide an illustrative example only: data are currently lacking as to the extent to which the ocean of Europa or any other moon matches the conditions described in this paper (Melosh et al. 2004). For example, whilst the likely ranges of temperature and pressure of a given moon’s ocean can be estimated to be within the limits of applicability of a given formulation, the effect on sound speed (and especially absorption) of solutes within Earth’s well-characterized oceans is not simple, and speculation for extraterrestrial oceans would unnecessarily clutter this tutorial. To allow for a simple and short analytical solution, this paper will assume that the ionic properties of all the liquid water on the generic icy moon of this paper can be assumed to give the equivalent effect of setting $S = 35 \text{ g kg}^{-1}$ in Eq. (7). The choice is made to facilitate the tutorial calculations, since it eliminates terms in Eq. (7) that would obscure the simple calculations undertaken here without adding to the understanding gained from the example. The value of the fitting parameter α is especially important for deep water regions with small variations in temperature and ionic content. For the pressure range encountered across the generic icy moon ocean of this paper, the value for the fitting parameter α which most closely matches the predictions of the UNESCO equation is here taken to be $\alpha = 1.702 \times 10^{-6}$ (Leighton 2012).

As an example scenario, suppose that a probe is dropped to the seafloor (at depth $H = 100$ km below the water/ice interface) near to a region of a hydrothermal vent which has been emitting warm water. As it fell it recorded that, as a result of the vent, the temperature in the water column was constant at $0.2\text{ }^\circ\text{C}$ from the base of the ice until a distance of $L = 20$ km above the seafloor, below which the temperature rises steadily by $1\text{ }^\circ\text{C}$ per additional km of descent. One group of scientists believe that this is a very localized effect, and that the probe has fallen into a plume of hot water of no more than 100 m horizontal extent, either side of which there is cold water at $0.2\text{ }^\circ\text{C}$. Another group believe that the rise in temperature as one approaches the seabed will be uniform for up to 500 km horizontally from the probe's path.

Whilst it had been intended to use acoustics in later probes to explore the profiles of pressure, temperature and composition within the ocean and ice (with suitable constraints from other measurements), in this early probe acoustics had been incorporated only at the simplest level, in that the probe was equipped with a simple ultrasonic range-finder. During the descent, this range-finder was used to monitor the distance to the seabed from the two-way time of flight taken for the pulse to travel to the seabed, reflect off it, and return to the probe (much in the way the SODOR system worked on Titan's *Huygen's* probe; Zarnecki et al. 2005). It is first activated at the base of the ice shell, and simply records the two-way travel time until the echoes return to the probe which, if the sound speed profile is known, gives the range to the reflecting features.

Once the probe has reached the seabed, to resolve the above dispute it is proposed remotely to re-orientate the sonar beam (the transducer is mounted on an arm) so that the powerful ultrasonic beam points horizontally. It is a simple matter to calculate where (according to the flat world model) the ultrasonic beam should reach the base of the ice sheet (where myriad floating sensors have been released which could detect it) assuming the temperature profile is horizontally uniform. If the probe's path happened to be in a narrow thermal plume the ultrasonic pulse will arrive at the base of the ice shell a horizontal distance of 379 km from the probe. If the temperature profile the probe encountered during its descent is uniform over ranges of 500 km or more from the probe, the ultrasonic pulse will reach the base of the ice shell a horizontal distance of 250 km from the probe. The following calculation shows how these estimates are made.

Assume (until Sect. 4) that the hydrostatic pressure in the water is:

$$P_h = \rho_{ice}gh_{ice} + \rho_wgz, \tag{8}$$

The temperature profile (Fig. 5) is:

$$T/T_{ref} = 0.2, \quad 0 \leq z \leq (H - L) \tag{9}$$

$$T/T_{ref} = 0.2 + 20(z - H + L)/L. \quad (H - L) \leq z \leq H \tag{10}$$

Equation (10) models the circumstance if the temperature profile is not restricted to the plume but instead is horizontally uniform over ranges of 500 km or more from the probe. Substitution into Eq. (7) and applying the condition that equates to $S/S_{ref} = 35$, gives:

$$c/c_{ref} \approx 1450.1 + \alpha(\rho_{ice}gh_{ice} + \rho_wgz)/P_{ref}, \quad 0 \leq z \leq (H - L) \tag{11}$$

$$c/c_{ref} \approx 1450.1 + 92(z - H + L)/L + \alpha(\rho_{ice}gh_{ice} + \rho_wgz)/P_{ref}, \quad (H - L) \leq z \leq H \tag{12}$$

where (11) and (12) have been obtained using a linearized version of (7) (neglecting in this first order tutorial calculation the quadratic and cubic temperature terms in (7), though they

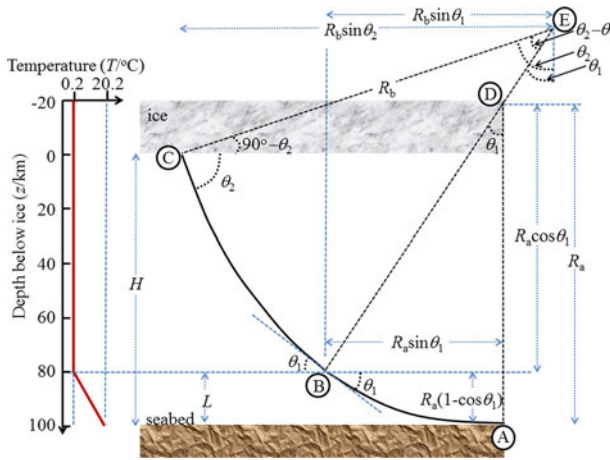


Fig. 5 Geometry of flat world ray tracing problem for rays emitted horizontally by probe on seabed into an ocean which has a thermal profile which is uniform in the horizontal direction but which has two distinct regions in the vertical profile (shown on the left). Whilst points A, B and C are defined to lie on the seabed, at the temperature profile discontinuity and at the water/ice interface, in general D and E will lie a considerable distance above the moon’s surface

are in fact respectively <30 and <4 % of the linear temperature term near the seabed, and very much less over most of the water column). As a result, the sound speed gradient is constant in the two regimes, i.e. there is a piece-wise linear model of sound speed. In addition, by construction, the two formulations [(11) and (12)] agree at the transition depth $z = H - L$, so that the sound speed profile is continuous at that point. For the particular example here, H is 100 km and L is 20 km and the sound speed at the transition depth ($z = 80$ km), is $1,669.5 \text{ m s}^{-1}$ (using $g = 1.31 \text{ m s}^{-2}$ which, until Sect. 4, will be assumed to be constant at all depths). Differentiation of (11) and (12) the with respect to z gives:

$$\frac{dc}{dz} \approx 0.00223 \text{ s}^{-1}, \quad 0 \leq z \leq (H - L) \tag{13}$$

$$\frac{dc}{dz} \approx 0.00683 \text{ s}^{-1}. \quad (H - L) \leq z \leq H \tag{14}$$

The radius of the raypath, R_a , as the ray travels in the regime $80 \leq z/\text{km} \leq 100$ can be computed using (6) as follows. The Snell’s law constant, c_0 , for this ray is equal to the sound speed when the ray is horizontal ($\theta = 0$) i.e. the depth of the probe, $z = 100$ km. The sound speed at 100 km depth is $1,806.1 \text{ m s}^{-1}$ [using (12)]. Combining this, in (6), with the sound speed gradient given in (14) leads to a radius for the raypath, R_a , of 264.4 km. The probe, at point A on Fig. 5, launches a signal which reaches point B at $z = 80$ km by travelling through an arc of radius R_a centred on point D (which in general will lie well above the planet’s surface). Applying Snell’s Law, the angle that the ray makes to the horizontal at $z = 80$ km is

$$\theta_1 = \cos^{-1} \left(\frac{c(z = 80 \text{ km})}{c(z = 100 \text{ km})} \right) \approx 22.4^\circ. \tag{15}$$

Since from (11) the sound speed in the water at the base of the ice shell is $c(z = 0 \text{ km}) \approx 1,491.1 \text{ m s}^{-1}$, then applying Snell’s law gives the angle that the ray makes to the horizontal at the ice/water interface (point C) to be

$$\theta_2 = \cos^{-1} \left(\frac{c(z = 0 \text{ km})}{c(z = 100 \text{ km})} \right) \approx 34.4^\circ. \tag{16}$$

The signal travels from point B to point C via an arc of radius R_b centred on point E. The radius of the raypath in the region $0 \leq z/\text{km} \leq 80$ is simply found because the constant c_0 is the same as it was during the ray propagation in the region $80 \leq z/\text{km} \leq 100$ ($1,806.1 \text{ m s}^{-1}$) and the sound speed gradient is that defined in (13), so that $R_b = 809.9 \text{ km}$. From Fig. 5, the horizontal distance covered when the ray travels from B to C in an arc of radius R_b centred on point E is $R_b(\sin \theta_2 - \sin \theta_1)$. Therefore the total horizontal distance from the probe to the point where the pulse meets the ice is $R_b(\sin \theta_2 - \sin \theta_1) + R_a \sin \theta_1 \approx 250 \text{ km}$. If the rise in temperature at depth of greater than $z = 80 \text{ km}$ were indeed to have been a localized anomaly that extended no more than around 50 m in the horizontal direction from the probe, then the horizontal distance from the probe at which the signal would reach the base of the ice shell is readily estimated, assuming that the refraction in that first 50 m is negligible. Here $c'(z)$ represents this alternative sound speed profile. The sound speed gradient is $dc'/dz \approx 0.00223 \text{ m s}^{-1}$, see (13), although now it applies throughout the water column. The Snell's law constant, c_0 , for this ray is equal to the sound speed at the base of the water column, and using (11) this is $1,714.1 \text{ m s}^{-1}$. The radius of curvature R' of the ray throughout its entire path in the water column would [from (6)] have been 768.6 km . From Snell's Law the angle of the ray to the horizontal when it reached the base of the ice shell would have been:

$$\theta' = \cos^{-1} \left(\frac{c(z = 0 \text{ km})}{c'(z = 100 \text{ km})} \right) \approx 0.516 \text{ radians (equivalent to } 29.55^\circ). \tag{17}$$

As a check, $H = R'(1 - \cos \theta')$, and the horizontal distance from the probe to the point where the ray reaches the base of the ice shell is $R' \sin \theta' \approx 379 \text{ km}$. The acoustic signal has travelled an arc distance of around $R'\theta' \approx 396 \text{ km}$ and taken around 250 s to sample the ocean temperature profile to a range of several hundred km around the probe (White et al. (2006) illustrate how the precise times can be calculated). Of course the answer is not unique, but in reality when this is done the acoustic signals are launched at a range of angles and as data from more paths are combined, the uncertainty in the estimate generally decreases. This will be explored further in Sect. 4.

One limitation of the flat world model is immediately apparent. If the distance from the centre of the generic icy moon to the base of the icecap in this model is $R_{\text{ice}} = 1,540,800 \text{ m}$, then an illustrative arc distance of 379 km horizontally on the curved base of the icecap would mean an arc angle of $379,000/1,540,800 \sim 0.246 \text{ radians}$ or 14° . Two points separated by an arc angle of 14° on the base of the generic moon's ice shell, would have a straight-line separation of $2R_{\text{ice}} \sin 7^\circ \approx 375.6 \text{ km}$ which differs from 379 km by 3.4 km . Although small on the scale of the above thought-experiment, such errors become larger with increasing range, reaching levels of absurdity in the circumpropagation experiments of Sect. 4.

4 Results for Curved Worlds

The geometrical error that occurs when applying the flat world model discussed so far in this paper that was illustrated at the end of Sect. 3, is compounded by more subtle problems when using such flat world models in the kind of acoustical problems discussed in Sect. 3.

They show up most plainly in the error inherent in the statement of Eq. (8). Potential deviations from sphericity and horizontal gradients have been shown to have a profound effect on Earth, as proven by Munk et al. (1988), though without use of the exact integral of $\nabla P_h = \rho_w g$. Section 4 explores these effects in circumpropagation scenarios further, using the methods of Leighton et al. (2008b).

4.1 Are the Discrepancies in Sound Speed Profile Significant?

The method of Leighton et al. (2008b) can be used to consider the effect on the propagation of using different temperature values for the homogeneous isothermal ocean which exists beneath the icy surface of the generic spherical moon modelled here. Given sufficient computational resources, the principle can extend to various temperature distributions and moon shapes. To calculate the oceanic sound speed profile, test values from 0 to 10 °C in steps of 1 °C were used for illustrative purposes (and should not be taken to represent our opinion of actual conditions on any particular moon). The value of α used throughout this section is $\alpha = 1.74 \times 10^{-6}$, as used by Leighton et al. (2008b) (sensitivity to the value of α is discussed by Leighton 2012). As before, to allow for simple calculations in the absence of data to the contrary, this paper will assume that the ionic properties of the water throughout the water column in this generic icy moon give the equivalent effect of setting $S = 35 \text{ g kg}^{-1}$ in Eq. (7).

Figure 6 shows three of these sound speed profiles (0, 4 and 10 °C), through an ocean which is assumed to be 100 km deep under 20 km of ice. The coordinate $z = 0$ represents the sea-ice interface, which is assumed to be perfectly smooth and reflecting. For each temperature, two sound speeds are shown: the solid line shows the sound speed calculated after the manner described in Leighton et al. (2008b); the broken line shows the sound speed calculated if the planet curvature is ignored, and the gravitational acceleration is taken to be equal to that at the planet's surface (1.31 m s^{-2}). It is the solid line profile that is used for the subsequent ray tracing calculations.

The difference between solid and broken lines in the value of the sound speed at the base of the water column, for a given temperature, is around 2 %, which raises the immediate question of whether such corrections are significant. It might be argued that this is small compared with the uncertainties in the parameter values which are used as input to the calculations. Such arguments however need to be critically assessed with care, as they are based on a misleading comparison between the systematic sound speed discrepancies shown in Fig. 6, and the current uncertainties in the values of other parameters (e.g. ocean temperature and ionic variations) whose physics is incorporated into the models (as accurately as our knowledge allows) but whose values are estimated with uncertainty. This is because one weakness of acoustic inversion techniques is that it can be difficult to assess the correctness of the result obtained by such an inversion: the fact that the inversion has been conditioned sufficiently to converge upon an answer does not mean that the answer is itself correct. If the inversion is based on a model which contains significant systematic errors in the physics, the answer to which it converges may be incorrect and misleading. The 2 % error in the broken lines of Fig. 6 do not represent random errors, or uncertainties in the value of input parameters, but rather they represent systematic errors in the physical model for propagation.

Leighton et al. (2008b) showed that neglect of planetary curvature and the variation of gravitational acceleration generated an error of $\sim 100 \text{ km}$ in the distance from the source to the first bounce at the water/ice interface after propagation through the upwardly-

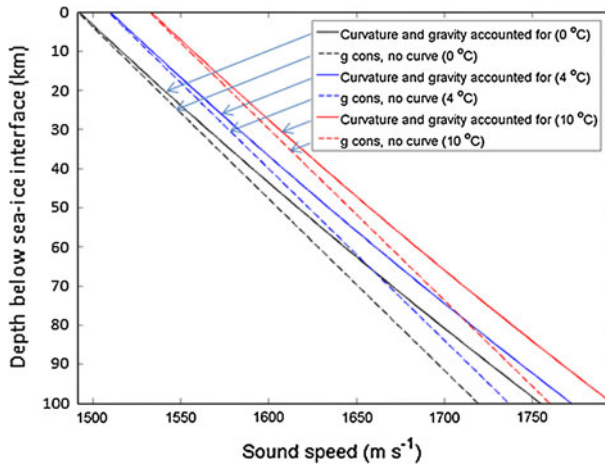


Fig. 6 Sound speed profiles for homogeneous ocean temperatures of 0, 4 and 10 °C. The oceanic sound speed is calculated as a function of depth beneath the base of the ice sheet, assuming an ionic content which has the same effect on the sound speed as would a salinity of $S = 35 \text{ g kg}^{-1}$, and constant densities for water ($\rho_w = 1,000 \text{ kg m}^{-3}$), ice ($\rho_{\text{ice}} = 920 \text{ kg m}^{-3}$) and using a spatially-averaged density of the seabed, mantle and core of $\rho_E = 3,550 \text{ kg m}^{-3}$. For each temperature, the *solid curve plots* the sound speed calculated including planet curvature and variable gravitational acceleration (see Leighton et al. 2008b for details). Also for each temperature, the *dashed curve plots* the sound speed calculated ignoring planet curvature and using for the gravitational acceleration a constant value of 1.31 m s^{-2} (the value at the moon's surface)

refracting water column (the error is reduced by half if planetary curvature is only neglected in the calculation of hydrostatic pressure but included elsewhere, e.g. in the curvature of the water/ice boundary). For the ray in question a 100 km discrepancy represented an error of nearly 20 %. This is not an insignificant distance on the scale of the problems considered: as Lee et al. (2003) comment regarding Europa, “A consistent estimate of the spatial separation between cracking events would be the roughly 100-km scale of a cycloidal feature (Hoppa et al. 1999)”.

Leighton et al. (2008b) noted that if small discrepancies in the modelling cause the character of the propagation to change qualitatively, the effect can be more significant than the percentage changes implied above. A simple example would be if a ray which would have refracted without intersecting off the seabed were instead (because of a slight change in sound speed profile) to reflect off the seabed. The sequence of acoustic arrivals at a remote location is then changed qualitatively as the pattern of multipaths is affected. The importance of the correct modelling of the qualitative ray paths when quantitatively predicting acoustic travel times is clear if circumstances are such that a small change in the assumed ocean temperature or depth can lead to an unexpectedly greater proportional change in travel time because it alters the number of reflections at the water-ice interface required for a specific return. This effect is demonstrated in a simple circumpropagation example in the next section.

4.2 A Simple Circumpropagation Example

The scenario to be considered is the case of rays generated from a given point on the generic icy moon, and propagating right around the moon once only to return to the point of origin. The rays which do this most quickly will take only one circumpropagation to

return to their point of origin. Clearly only some ray paths will achieve this in one single circumpropagation: others will take more time, and arrive later. Given the restrictions cited above on which oceanic acoustic waves are being considered, this subsection will illustrate how the first arrival will correspond to the ray path which returns to its source after a single circumpropagation, and does this whilst penetrating to the deepest ocean depths (Fig. 7).

Consider only those ray paths which propagate through the water (rays which reflect off the base of the ice sheet must necessarily be considered for long range acoustic propagation in an upwardly refracting ocean, but rays which interact with the seabed or which travel through the ice are not considered in this simple illustration, and will be neglected throughout this paper). Of these rays, the one which travels to great distances in the least time is that ray which penetrates the deepest and so just grazes the seabed. This is because although the path length for this ray is long compared to others, this deep path takes the ray through the aqueous regions where the sound speed is the greatest. This is illustrated through the following numerical example. Consider the three rays shown in Table 1, which records the case when $R_{\text{ice}} = 1,540.8$ km, and $R_{\text{bed}} = 1,440.8$ km, with an ocean temperature of $T = 0$ °C. Those rays are launched at angles below the horizontal of 36.1° , 34.1° and 37.5° .

From Table 1, the ray launched at 36.1° would, by the criteria used in this paper, be taken as having the largest launch angle that completes an integer number of bounces. It is understood that the ray approach is an inexact analogy for sound propagation, but we may consider this deepest ray as indicating the approximate position of the deepest part of the wavefront to complete circumpropagation without reflecting off the seabed. All calculations in this report are of course approximate because of the limitations of numerical accuracy in such calculations (see footnote 2).

We then explore the properties of the next deepest, and next most shallow, rays to complete circumpropagation once using an integer number of bounces.

The ray launched at 34.1° would be, by the manner of calculation used in this report, the next ray which requires an integer number of bounces (i.e. the one which would be deepest were it not for the ability of the 36.1° ray to complete circumpropagation in an integer number of bounces without reflecting off the seabed). It takes longer to circumpropagate

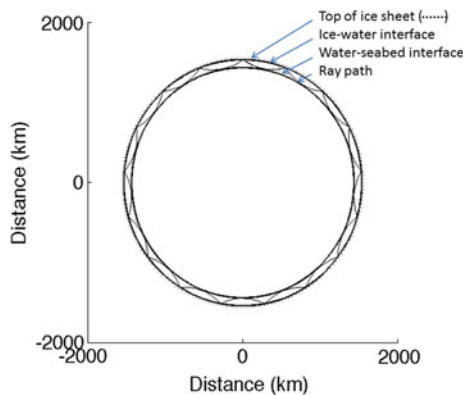


Fig. 7 This plot depicts the path followed by the first ray which will circumnavigate the generic icy moon sea were the water to be isotropic at 0 °C (considering only those acoustic rays which propagate in the water and which reflect off the water–ice interface). The ray is launched at an angle of 36.1° below the horizontal, and arrives at the starting point after grazing the ocean bottom 17 times. The value of R_{ice} is 1,540,800 m. The image is approximately to scale

Table 1 Propagation characteristics for three rays launched at angles below the horizontal of 36.1°, 34.1° and 37.5°, for $R_{ice} = 1,540.8$ km, and $R_{bed} = 1,440.8$ km, and an ocean temperature of $T = 0$ °C

Launch angle	Number of bounces	Time (mins)	Distance (Mm)
36.1	17	101.07	9.975
34.1	18	101.82	9.940
37.5	18	102.21	10.110

because its path avoids the deeper waters where the sound speed is greatest. Note the 34.1° ray takes a shorter path but through a slower part of the ocean, compared to the 36.1° ray.

The ray launched at 37.5° reflects from the seabed and requires an integer number of complete bounces (a complete bounce is when the ray returns to the surface). Its '18 bounces' to complete circumpropagation may be thought of as consisting of 36 half-bounces, a half-bounce consisting of a path between ice and seabed, or vice versa.

In the following two subsections, two cases are explored. Section 4.3 discusses the effect on the earliest through-water circumpropagating arrival of changes in the position of the water/ice interface for a fixed ocean temperature. Section 4.4 changes in the ocean temperature for a fixed water/ice interface.

The calculations of Sects. 4.3 and 4.4 are important steps in building the argument for multipath inversion, which will be made in Sect. 5. On their own, they do not represent realistic experiments: global ocean temperature changes, and changes in the water-ice boundary uniformly over a spherically symmetric world without compensatory changes, are highly unlikely, and no useful inversion would be undertaken using the arrival time of a single ray (the first arrival) since the inversion would be ill-conditioned (multiple solutions to explain the arrival time of a single ray, trading off water temperature against ice thickness for example). They are presented here not as possible experiments, but as the penultimate step in the tutorial process.

4.3 The Effect of the Position of the Water/Ice Layer

Over its history, there are many forces which influence the position of the ice/water layer within icy moons (Spohn and Schubert 2003; McKinnon 2006). The icy moon model used in this paper is spherically symmetric, and for most processes the timescales over which the water/ice layer moves in a spherically symmetric manner would not fall within the limited period of observation of a probe on the ice designed to receive (and possibly emit) acoustic signals. As such, the model tested here of variations in the ice/water boundary for a spherical moon are unlikely to be germane in their own right. However here they are used as a simple proxy for assessing departures from sphericity during orbit. The effect of rotation and tides causes departures from sphericity (VanHoolst et al. 2008), and a suitable inversion based on multipath propagation with ancillary data could monitor these changes, particularly if the orbital changes triggered a 'toggle point' discontinuity (see later).

In contrast to the dimensions stated in Sect. 2.1, where the water/ice interface is assumed to be fixed, this section will explore the effect of altering the exact position of the water/ice interface (i.e. changing h_{ice} and R_{ice} whilst keeping $R_{outer} = 1,560,800$ and $R_{bed} = 1,440,800$ m constant), on the understanding that this artificial situation represents the penultimate stage in the tutorial before full multipath inversion is discussed.

Figure 7 shows one example of a circumpropagating ray which is the first to complete through-water circumpropagation of the generic icy moon ocean under ice for the stated conditions. As with all the cases to be discussed in this subsection, the model assumes that the ocean temperature is uniform at 0 °C (again, just for convenience as it simplifies the form of Eq. 7). This, the first of the rays to return to the point of origin after a single circumpropagation, does so by reflecting off the ice 16 times, and arrives at the starting point after grazing the ocean bottom 17 times. It is the ray which left the source (assumed to be at the base of the ice sheet) at an angle of 36.1° (to three significant figures) below the local horizontal (in practice, even highly directional sources have beams of finite angular extent).

The propagation path lengths and times for the rays which just graze the seabed (and which undertake the most rapid through-water circumpropagation) are shown in Table 2 for the convenient artifice of assuming constant ocean temperature and constant values for the position of the seabed and the outer radius of the planet (i.e. the top of the ice sheet), as the position of the water/ice layer changes in 1 km increments.

As the ice thickness³ increases incrementally from 14 to 25 km, the propagation time decreases monotonically (obviously this is an idealised model, and departures from sphericity and environmental inhomogeneities will cause significant perturbations). However between ice thicknesses of 12 and 13 km, the propagation time for the first circumpropagating ray increases by nearly 49 s. This ‘toggle point’ transition occurs because the propagation path undergoes qualitative changes, with respect to the number of reflections of the water/ice interface which the earliest through-water circumpropagating ray requires. Between ice thicknesses of 26 and 27 km, the travel time for the first through-water arrival undergoes another large discontinuous increase by over 40 s. Like the one which occurred between ice thicknesses of 12 and 13 km, this discontinuity also occurs because of an increase by one in the number of reflections required for circumpropagation by the ray which grazes the seabed. Figure 8 plots the travel time against the ice thickness shown in Table 2. Figure 9 shows, for each ice thickness, what the change in travel time for the most rapid through-water circumpropagation would be were the ice thickness to increase by 1 km.

4.4 The Effect of the Ocean Temperature

Table 3 plots the propagation characteristics for the most rapid through-water ray to circumpropagate the moon and return to source [for the generic spherical icy moon with uniform material properties, including a fixed sea floor ($R_{\text{bed}} = 1,440,800$ m), external radius ($R_{\text{outer}} = 1,560,800$ m), and a fixed position for the water/ice interface ($R_{\text{ice}} = 1,534,000$ m)]. This is done as the uniform ocean temperature varies in increments of 1 °C from 0 to 10 °C (chosen for the numerical illustration only, and not implying the existence of any particular ocean temperature profile in reality).

A ‘toggle point’ occurs between 1 and 2 °C (Fig. 10), in that a change occurs in the number of bounces required to circumpropagate the moon and return to source. The qualitative change in the propagation pattern generates an effect which is proportionally much greater than would occur away from a toggle point (Fig. 11).

This example illustrates how a change in the qualitative feature in the acoustic propagation can greatly increase the change in an observable far beyond any presupposed linear

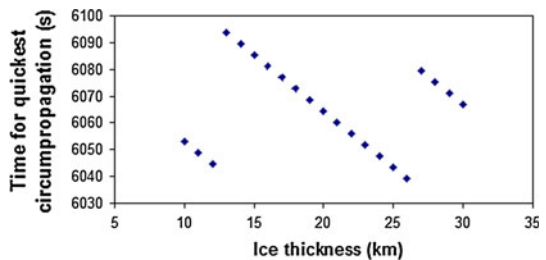
³ Note that in this artificial calculation, the effect of changing ice thickness on the through-water propagation time is an indirect one, resulting from the fact that, for fixed R_{bed} and R_{outer} , any change in ice thickness perforce requires a change in the thickness of the water column.

Table 2 For the generic spherical icy moon of this paper with uniform material properties, for a fixed sea floor ($R_{bed} = 1,440,800$ m) and external radius ($R_{outer} = 1,560,800$ m) and a uniform ocean temperature of 0 °C, the characteristics of the earliest-arriving through-water circumpropagating ray are tabulated as a function of the radius of the base of the ice sheet (R_{ice}), which is discretely changed in 1 km increments

Ice thickness (km)	Radius of the base of the ice sheet (R_{ice}/km)	Ray angle at release from source (degrees)	Number of times the ray grazes the seafloor during one circumpropagation	Travel time (s)	Path length (Mm)
10	1,550.8	38.2878	16	6,053.1	10.0804
11	1,549.8	38.2893	16	6,048.9	10.0739
<i>12</i>	<i>1,548.8</i>	<i>38.2907</i>	<i>16</i>	<i>6,044.8</i>	<i>10.0675</i>
<i>13</i>	<i>1,547.8</i>	<i>36.0842</i>	<i>17</i>	<i>6,093.6</i>	<i>10.0197</i>
14	1,546.8	36.0855	17	6,089.4	10.0133
15	1,545.8	36.0868	17	6,085.2	10.0068
16	1,544.8	36.0881	17	6,081.0	10.0004
17	1,543.8	36.0894	17	6,076.9	9.9940
18	1,542.8	36.0908	17	6,072.7	9.9876
19	1,541.8	36.0921	17	6,068.5	9.9811
20	1,540.8	36.0935	17	6,064.3	9.9747
21	1,539.8	36.0949	17	6,060.1	9.9683
22	1,538.8	36.0964	17	6,056.0	9.9618
23	1,537.8	36.0978	17	6,051.8	9.9554
24	1,536.8	36.0993	17	6,047.6	9.9490
25	1,535.8	36.1007	17	6,043.4	9.9426
26	<i>1,534.8</i>	<i>36.1022</i>	<i>17</i>	<i>6,039.2</i>	<i>9.9361</i>
27	<i>1,533.8</i>	<i>34.1326</i>	<i>18</i>	<i>6,079.3</i>	<i>9.8959</i>
28	1,532.8	34.1339	18	6,075.1	9.8895
29	1,531.8	34.1353	18	6,070.9	9.8831
30	1,530.8	34.1367	18	6,066.7	9.8767

Two pairs of adjacent rows (for ice thicknesses of 12 and 13 km, and 26 and 27 km) are italicised, indicating the ‘toggle point’ where, for these ocean parameters, the 1 km incremental change in the position of the water/ice interface changes the number of reflections required to complete the earliest through-water circumpropagation. The ocean geometry (for ice thickness 26.8 km) is close to the toggle point which occurs between 26 and 27 km ice thickness. Throughout this paper, the precision to which values are calculated is not meant to reflect their accuracy, but rather the caution used in these preliminary calculations before the magnitude of the effects at the toggle points has been evaluated

Fig. 8 Plot of the travel time for the earliest-arriving through-water circumpropagating ray which returns to the position of the source, as a function of the thickness of the ice (data from Table 2)



relationship. Furthermore it points to ways in which such observables could be exploited to provide more sensitive measurements of the ocean environment. Whilst the heterogeneity and bathymetry of the ice seas of Earth and the icy moons are vastly more complicated

Fig. 9 For each ice thickness, the vertical axis shows what would be the change in travel time for the most rapid through-water circumpropagating ray, were the ice thickness to increase by 1 km (using the data from Table 2)

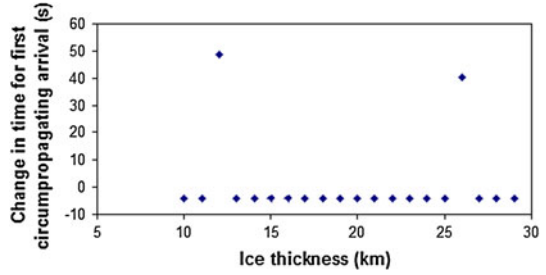
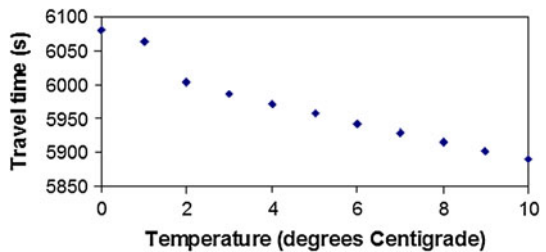


Table 3 For the generic spherical icy moon of this paper with uniform material properties [for a fixed sea floor ($R_{bed} = 1,440,800$ m), external radius ($R_{outer} = 1,560,800$ m), and for fixed position of the water/ice interface ($R_{ice} = 1,534,000$ m) and a fixed ice thickness of 26.8 km], the propagation characteristics are tabulated for the most rapid through-water ray to circumpropagate the moon and return to source

Temperature (°C)	Number of times the ray grazes the seafloor during one circumpropagation	Launch angle (degrees)	Travel time (s)	Distance (Mm)
0	18	34.13	6,080.4	9.8972
<i>1</i>	<i>18</i>	<i>34.07</i>	<i>6,063.0</i>	<i>9.8955</i>
2	17	35.97	6,003.0	9.9272
3	17	35.90	5,987.4	9.9252
4	17	35.84	5,971.8	9.9235
5	17	35.78	5,957.4	9.9218
6	17	35.72	5,943.0	9.9201
7	17	35.66	5,928.6	9.9184
8	17	35.60	5,915.4	9.9168
9	17	35.55	5,902.2	9.9153
10	17	35.49	5,889.6	9.9137

This is done as the uniform ocean temperature varies in increments of 1 °C from 0 to 10 °C (chosen for the numerical illustration only, and not implying the existence of any particular ocean temperature on any given moon). As with Table 2, the pair of rows that are italicized indicate the occurrence of a ‘toggle point’

Fig. 10 The travel time for the most rapid through-water ray to circumpropagate the moon and return to source, plotted as a function of the ocean temperature, using the data of Table 3



than those assumed in the simple model of this study, the existence of toggle points could provide useful indicators of environmental change even at shorter ranges than those required for circumpropagation.

Inversions based on the arrival time of the first ray are however insufficient to provide a unique answer unless a sufficient number of environmental parameter values have been confirmed by alternative means. For example, an observed first arrival circumpropagation time of ~6,050 s could correspond to an ice thickness is of ~11 or ~24 km with a

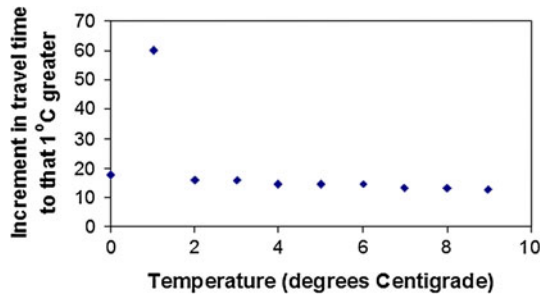


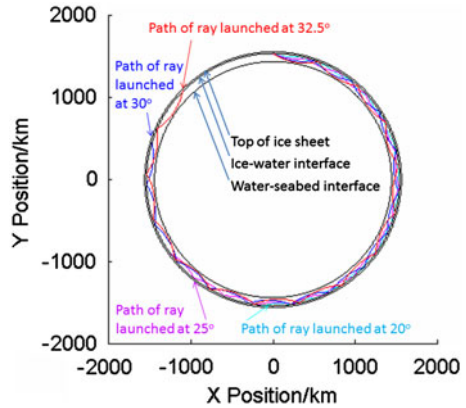
Fig. 11 For each ocean temperature cited on the abscissa, the value on the mantissa shows the change in travel time (for the most rapid through-water ray to circumpropagate the moon and return to source) between the travel time at the cited temperature, and the travel time at a temperature of 1 °C greater. Data obtained from Table 3

temperature of 0 °C (see Fig. 8) or ~ 26.8 km with a temperature of about 1.5 °C (Fig. 10). Even in a spherically symmetric world, the single observable of travel time for the first arrival cannot be interpreted if enough environmental variables have not been tied down using independent measurements. In general, the greater the number of unknowns, the more data need to be used as input to the inversion. Fortunately, in the case of acoustic propagation in icy moons, considerable data in addition to the first arrival time is available through the energy which propagates along other paths to the receiver each time the source emits a signal. Their nature will be discussed in the conclusion to this tutorial.

5 Conclusions

This paper introduces key concepts in using long range acoustic propagation to monitor an ocean environment. It considers a model of a generic icy moon's ocean and within it generates sound speed profiles to consider the paths of those acoustic rays which propagate through the water, but which only interact with the ice-water interface. The model of the moon itself is very much simplified, in that the moon is assumed to be spherically symmetric, and is divided up into three types of material (water, ice and other material), such that at any given radius only one type of material occurs, and it has uniform density wherever that material occurs on the moon. The key acoustical finding (that raypaths follows the arcs of circles if the sound speed gradient is linear) is used in simple 'flat world' examples, which are then criticized for failure to take into account planetary curvature, variation of g with depth, and inappropriate integration of $\nabla P_h = \rho_w g$ to obtain the contribution to hydrostatic pressure by the water column. The extreme example of when these factors must be taken into account (circum-propagation) was used to illustrate the position of 'toggle points', discontinuities in the travel time for the first arrival ray as the environment changes monotonically. However two issues remain: first, the nature of the monotonic changes (changes due to orbits around planet and sun are more likely than spherically symmetric changes to water temperature and water/ice interfaces); second, without sufficient constraints through independent measurements of environmental parameters, such calculations cannot be inverted (an ambiguity between ice thickness and water temperature in inferring the environment from the first arrival time was shown at the end of Sect. 4). However all the examples shown in Sects. 3 and 4 consider the arrival of one ray. The real value of the technique comes when the range of raypaths that might be detected is considered. A single emission produces a sequence of arrivals corresponding to

Fig. 12 Rays emitted at 20°, 25°, 30°, and 32.5° below the horizontal propagate from a source at the water/ice interface. Each ray has been traced here for 13 reflections. The image is approximately to scale



different multipaths, and discontinuous changes to that sequence become sensitive change detectors e.g. if the moon changes the degree of asphericity during orbit. Europa is known to have the shape of a tri-axial ellipsoid with radii ζ_a , ζ_b and ζ_c such that at the surface the equatorial flattening ($\zeta_b - \zeta_a$) is of ~ 2.4 km and the polar one ($\zeta_c - \zeta_a$) is ~ 3.2 km.

Figure 12 plots the paths of rays in the generic icy moon ocean from a range of launch angles from a source at the water/ice interface. These calculations have a vertical axis of rotational symmetry for assumed conditions. The various rays will propagate around the world, and a subset of these will be detected at a remote sensor. Ignoring waves that propagate wholly or in part through the ice and seabed, the number detected will depend of the beamwidth and how it spreads, and some rays may take several circumpropagations before they reach the detector (signal-to-noise ratio allowing). Hence the sequence of arrivals might be schematically illustrated on Fig. 13a, where the earliest arrivals (corresponding to the deepest ray paths if for the moment we restrict ourselves to through-water propagation only) are infrequent, but as time progresses during the first tranche of arrivals (those which only require one circumpropagation to return to source), the later arrivals occur more frequently. The simple example illustrated in Fig. 13 shows that the measured late arrivals within the first tranche agree with the predictions, indicating that the temperature in the model for ray paths restricted to shallow waters just beneath the icecap, are correct. However the predicted early arrivals are slower than the measured ones, indicating that the temperature close to the seabed differs from that assumed in the model (and is probably warmer).

It is of course entirely appropriate to question the value of this current study, given the extreme simplifications involved in the current model. The results shown here are intended to be indicative,⁴ but that does not make them without value. The moon will depart from spherical symmetry, and from the simple model of three homogeneous material types, each material having an unvarying density and temperature wherever it occurs. However the modelling in Tables 2 and 3 is calculated by considering single arcs, and multiplying the effect to obtain results for circumpropagation: departures in spherical symmetry would be revealed by arc-to-arc variations, if sufficient sensors could be deployed to detect these, and could provide a valuable diagnostic tool for the ocean environment.

The example of circumpropagation is somewhat artificial: a sound source which is sufficiently loud to generate a signal that is detectable above the noise and reverberation after

⁴ Repeated calculations, setting up the numerical scheme in different independent ways, showed that the toggle points in Tables 2 and 3 could shift by ± 1 km or ± 1 °C. However the object of this study is to draw attention to their existence and trends, not to the exact values of the output.

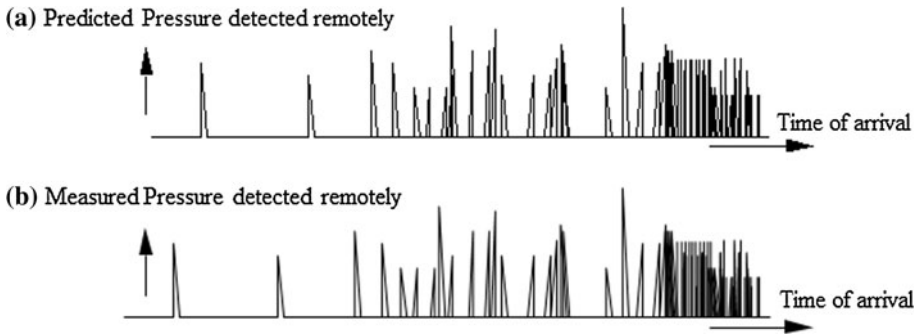


Fig. 13 Schematic showing the arrival times of pressure pulses detected at a point that is remote from the source, specifically the first tranche of arrivals to be detected at the position of the source after completing one circumpropagation only through the water column (other paths, and later tranches corresponding to multiple circumpropagations, are neglected). Comparison of panels (a) and (b) illustrates the case where the late arrivals are observed at the times predicted by the code, but where the early arrivals are detected prematurely in comparison with the numerical predictions

circumpropagating around the planet would, if naturally produced by collision or ice fracture, have resulted from such an energetic event that the measurement site itself could conceivably have been destroyed. However a focus point for sound at the moon's point diametrically opposite to the source would occur in the model used here, and in the idealised model the contribution to attenuation caused by geometrical spreading losses will be reversed as signals converge towards the source or its diametric pole.

Another simplification in this model is found in the simple specular reflections from the sea-ice interface, and the lateral homogeneity of the sound speed profile. These are not likely to be found in a real icy moon such as Europa (the base of the ice sheet will be shaped and may contain bubbles). However the calculations undertaken in this paper were not done to provide accurate predictions for experimental conditions on any given icy moon, but rather to show the trends and potentials for through-water propagation on that moon. If round-planet propagation can be predicted, then shorter ranges which are nevertheless sufficiently great for meaningful inversions, are feasible. Extension of such long-range propagation techniques to include seismic and other waves in the ice and mantle, and application to other bodies, would need consideration for a practical inversion.

It is important to recall that the scope of any equipment which is eventually placed on Europa will be limited, so that whilst in principle it is possible to determine far more from long-range propagation than these calculations suggest, equipment limitations will restrict the observations. For example, whilst the angle of propagation of each ray in the ocean could be determined using a hydrophone array in the water column, such a deployment would be extremely difficult. This study has restricted itself to simple direct observables, and if the limited equipment payload for Europa is to be optimised, quantitative studies of what can be achieved with limited resources are an important component of planning.

References

- M.A. Ainslie, T.G. Leighton, Near resonant bubble acoustic cross-section corrections, including examples from oceanography, volcanology, and biomedical ultrasound. *J. Acoust. Soc. Am.* **126**(5), 2163–2175 (2009)
- J.D. Anderson, G. Schubert, R.A. Jacobson, E.L. Lau, W.B. Moore, W.L. Sjogren, Europa's differentiated internal structure: inferences from four Galileo encounters. *Science* **281**(5385), 2019–2022 (1998)

- W.W.L. Au, S.W. Martin, Why dolphin biosonar perform so well in spite of mediocre “equipment”. *IET Radar Sonar Navig.* **6**(6), 566–575 (2012)
- H. E. Bass, H. Yan, Passive acoustic tornado detector and detection method. United States Patent 5355350 (1994)
- C. Béghin, C. Sotin, M. Hamelin, Titan’s native ocean revealed beneath some 45 km of ice by a Schumann-like resonance. *C.R. Geosci.* **342**, 425–433 (2010)
- D. Brecht, L. Ginzkey, Contribution to the hydroacoustic ocean monitoring of the UN Test Ban Treaty; signal classification by an autonomous buoy system. *J. Acoust. Soc. Am.* **107**(2), 1049–1052 (2000)
- C.-T. Chen, F.J. Millero, Speed of sound in seawater at high pressures. *J. Acoust. Soc. Am.* **62**, 1129–1135 (1977)
- A. Cook, V. Masek, in *The SEAformatics Project: Empowering the Seafloor*. Proceedings of the OCEANS 2009, MTS/IEEE Biloxi—Marine Technology for Our Future: Global and Local Challenges, 26–29 Oct 2009. Print ISBN: 978-1-4244-4960-6 (2009)
- G.D. Crawford, D.J. Stevenson, Gas driven water volcanism in the resurfacing of Europa. *Icarus* **73**, 66–79 (1988)
- G.T. Delory, J.G. Luhmann, D.W. Curtis, L.D. Friedman, J.H. Primbsch, F.S. Mozer, in *Development of an Audio Microphone for the Mars Surveyor 98 Lander*. Proceedings of the First International Conference on Mars Polar Science and Exploration, Lunar and Planetary Institute Contributions, **953**, 6 (1998)
- B.D. Dushaw, P.F. Worcester, W.H. Munk, R.C. Spindel, J.A. Mercer, B.M. Howe, K. Metzger Jr, T.G. Birdsall, R.K. Andrew, M.A. Dzieciuch, B.D. Cornuelle, D. Menemenlis, A decade of acoustic thermometry in the North Pacific Ocean. *J. Geophys. Res.* **114**, C07021 (2009). doi:[10.1029/2008JC005124](https://doi.org/10.1029/2008JC005124)
- N.P. Fofonoff, R.C. Millard, Jr., Algorithms for computation of fundamental properties of seawater. UNESCO Technical Papers in Marine Science No. 44, endorsed by UNESCO/SCOR/ICES/IAPSO Joint Panel on Oceanographic Tables and Standards and SCOR Working Group 51, UNESCO (1983)
- M.R. Frank, C.E. Runge, H.P. Scott, S.J. Maglio, J. Olsoa, V.B. Prakapenka, G. Shen, Experimental study of the NaCl–H₂O system up to 28 GPa: implications for ice-rich planetary bodies. *Phys. Earth Planet. Inter.* **155**(1–2), 152–162 (2006)
- M. Fulchignoni, F. Ferri, F. Angrilli, A.J. Ball, A. Bar-Nun, M.A. Barucci, C. Bettanini, G. Bianchini, W. Borucki, G. Colombatti, M. Coradini, A. Coustenis, S. Debei, P. Falkner, G. Fanti, E. Flamini, V. Gaborit, R. Gard, M. Hamelin, A.M. Harri, B. Hathi, I. Jernej, M.R. Leese, A. Lehto, P.F. Lion Stoppato, J.J. Lopez-Moreno, T. Mäkinen, J.A.M. McDonnell, C.P. McKay, G. Molina-Cuberos, F.M. Neubauer, V. Pirronello, R. Rodrigo, B. Saggin, K. Schwingenschuh, A. Seiff, F. Simoes, H. Svedhem, T. Tokano, M.C. Towner, R. Trautner, P. Withers, J.C. Zarnecki, In situ measurements of the physical characteristics of Titan’s environment. *Nature* **438**, 785–791 (2005)
- E.J. Gaidos, K.H. Nealson, J.L. Kirschvink, Life in ice-covered oceans. *Science* **284**(5420), 1631–1633 (1999)
- O. Grasset, C. Sotin, F. Deschamps, On the internal structure and dynamics of Titan. *Planet. Space Sci.* **48**(7–8), 617–636 (2000)
- R. Greenberg, Tides and the biosphere of Europa. *Am. Sci.* **90**, 48–55 (2002)
- R.N. Hadcock, R.R. Chipman, M. Horn, R.F. Chance, Integrated system for aircraft crack detection. US Patent 5,065,630 (1991)
- A. Hagermann, P.D. Rosenberg, M.C. Towner, J.R.C. Garry, H. Svedhem, M.R. Leese, B. Hathi, R.D. Lorenz, J.C. Zarnecki, Speed of sound measurements and the methane abundance in Titan’s atmosphere. *Icarus* **189**, 538–543 (2007)
- G.V. Hoppa, B.R. Tufts, R. Greenberg, P.E. Geissler, Formation of cycloidal features on Europa. *Science* **285**, 1899–1902 (1999)
- G. Hoppa, R. Greenberg, B.R. Tufts, P. Geissler, C. Phillips, M. Milazzo, Distribution of strike-slip faults on Europa. *J. Geophys. Res.* **105**(22), 617–628 (2000)
- H. Hussmann, F. Sohl, T. Spohn, Subsurface oceans and deep interiors of medium-sized outer planet satellites and large trans-neptunian objects. *Icarus* **185**, 258–273 (2006)
- L. Iess, R.A. Jacobson, M. Ducci, D.J. Stevenson, J.I. Lunine, J.W. Armstrong, S.W. Asmar, P. Racioppa, N.J. Rappaport, P. Tortora, The tides of Titan. *Science* 1219631 (Published online 28 June 2012). doi:[10.1126/science.1219631](https://doi.org/10.1126/science.1219631) (2012)
- F.B. Jensen, W.A. Kuperman, M.B. Porter, H. Schmidt, *Computational Ocean Acoustics* (Springer, New York, 2000)
- J. Jiang, K. Baik, T.G. Leighton, Acoustic attenuation, phase and group velocities in liquid-filled pipes II: simulation for spallation neutron sources and planetary exploration. *J. Acoust. Soc. Am.* **130**(2), 695–706 (2011)

- L. Ksanfomality, N.V. Goroschkova, V. Khondryev, Wind velocity near the surface of Venus from acoustic measurements. *Cosmic Res.* **21**, 161–167 (1983a)
- L.V. Ksanfomality, F.L. Scarf, W.W.L. Taylor, The electrical activity of the atmosphere of Venus, in *Venus*, ed. by D.M. Hunten, L. Colin, T.M. Donahue, V.I. Moroz (University of Arizona Press, Tucson, 1983b), pp. 565–603
- R.L. Kovach, C.F. Chyba, Seismic detectability of a subsurface ocean on Europa. *Icarus* **150**, 279–287 (2001)
- S. Lee, M. Zanolin, A.M. Thode, R.T. Pappalardo, N.C. Makris, Probing Europa's interior with natural sound sources. *Icarus* **165**, 144–167 (2003)
- S. Lee, R.T. Pappalardo, N.C. Makris, Mechanics of tidally driven fractures in Europa's ice shell. *Icarus* **177**, 367–379 (2005)
- I. Leifer, D. Tang, The acoustic signature of marine seep bubbles. *J. Acoust. Soc. Am.* **121**, EL35–EL40 (2007)
- T.G. Leighton, *The Acoustic Bubble* (Academic Press, London, 1994), p. 28
- T.G. Leighton, The use of acoustics in space exploration. ISVR Technical Report 314, University of Southampton (2007)
- T.G. Leighton, The use of extra-terrestrial oceans to test ocean acoustics students. *J. Acoust. Soc. Am.* **131**(3 Pt 2), 2551–2555 (2012)
- T.G. Leighton, A. Petculescu, The sound of music and voices in space. *Acoust. Today* **5**(3), 17–29 (2009)
- T.G. Leighton, P.R. White, Quantification of undersea gas leaks from carbon capture and storage facilities, from pipelines and from methane seeps, by their acoustic emissions. *Proc. R. Soc. A* **468**, 485–510 (2012)
- T.G. Leighton, A. Petculescu, Sounds in space: the potential uses for acoustics in the exploration of other worlds. *Hydroacoustics* **11**, 225–238 (2008)
- T.G. Leighton, P.R. White, M.F. Schneider, The detection and dimension of bubble entrainment and comminution. *J. Acoust. Soc. Am.* **103**(4), 1825–1835 (1998)
- T.G. Leighton, M. Farhat, J.E. Field, F. Avellan, Cavitation luminescence from flow over a hydrofoil in a cavitation tunnel. *J. Fluid Mech.* **480**, 43–60 (2003)
- T.G. Leighton, P.R. White, D.C. Finfer, in *The Sounds of Seas in Space*. Proceedings of the International Conference on Underwater Acoustic Measurements, Technologies and Results, 2005, eds. by J.S. Papadakis, L. Bjorno, pp. 833–840
- T.G. Leighton, F. Fedele, A. Coleman, C. McCarthy, S. Ryves, A. Hurrell, A. De Stefano, P.R. White, A passive acoustic device for real-time monitoring the efficacy of shockwave lithotripsy treatment. *Ultrasound Med. Biol.* **34**(10), 1651–1665 (2008a)
- T.G. Leighton, D.C. Finfer, P.R. White, The problems with acoustics on a small planet. *Icarus* **193**(2), 649–652 (2008b)
- T.G. Leighton, D.C. Finfer, G.-H. Chua, P.R. White, J.K. Dix, Clutter suppression and classification using twin inverted pulse sonar (TWIPS). *Proc. R. Soc. A* **466**, 3453–3478 (2010)
- T.G. Leighton, D.C. Finfer, G.-H. Chua, P.R. White, J.K. Dix, Clutter suppression and classification using twin inverted pulse sonar in ship wakes. *J. Acoust. Soc. Am.* **130**(5), 3431–3437 (2011)
- T.G. Leighton, J. Jiang, K. Baik, Demonstration comparing sound wave attenuation inside pipes containing bubbly water and water droplet fog. *J. Acoust. Soc. Am.* **131**(3) Part 2, 2413–2421 (2012)
- J.H. Lipps, S. Rieboldt, Habitats and taphonomy of Europa. *Icarus* **177**(2), 515–527 (2005)
- N.C. Makris, Probing for an ocean on Jupiter's moon Europa with natural sound sources. *Echoes* **11**(3), 1–3 (2001)
- N.C. Makris, S. Lee, A. Thode, J.D. Wilson, M. Zanolin, R.T. Pappalardo, Probing Europa's interior structure with natural ambient noise. American Geophysical Union, Fall Meeting 2001, abstract #P22B-0552 (2001)
- G.M. Marion, C.H. Fritsen, H. Eicken, M.C. Payne, The search for life on Europa: limiting environmental factors, potential habitats, and earth analogues. *Astrobiology* **3**(4), 785–811 (2003)
- B. Mason, Marine survey sees net gain in number of fish species. *Nature* **425**(6961), 889 (2003)
- W.B. McKinnon, On convection in ice I shells of outer Solar System bodies, with detailed application to Callisto. *Icarus* **183**(2), 435–450 (2006)
- H. Medwin (ed.), *Acoustical Oceanography: Sound in the Sea* (Cambridge University Press, New York, 2005)
- H. Medwin, C.S. Clay, *Fundamentals of Acoustical Oceanography* (Academic Press, San Diego, 1998), pp. 4–5
- H.J. Melosh, A.G. Ekholm, A.P. Showman, R.D. Lorenz, The temperature of Europa's subsurface water ocean. *Icarus* **168**, 498–502 (2004)

- P.N. Mikhalevsky, A.N. Gavrilov, Acoustic thermometry in the Arctic Ocean. *Polar Res.* **20**, 185–192 (2001)
- H. Muir, Sounds in space. *New Sci.* **195**(2616), 28–32 (2007)
- W.H. Munk, W.C. O'Reilly, J.L. Reid, Australia–Bermuda sound transmission experiment (1960) revisited. *J. Phys. Oceanogr.* **18**, 1876–1898 (1988)
- F. Nimmo, P. Schenk, Normal faulting on Europa: implications for ice shell properties. *J. Struct. Geol.* **28**, 2194–2203 (2006)
- F. Nimmo, P.C. Thomas, R.T. Pappalardo, W.B. Moore, The global shape of Europa: constraints on lateral shell thickness variations. *Icarus* **191**(1), 183–192 (2007)
- M. Panning, V. Lekic, M. Manga, F. Cammarano, B. Romanowicz, Long-period seismology on Europa: 2. Predicted seismic response. *J. Geophys. Res.* **111**, E12009 (2006)
- A. Petculescu, R.M. Lueptow, Atmospheric acoustics of Titan, Mars, Venus, and Earth. *Icarus* **186**, 413–419 (2007)
- N.J. Rappaport, L. Iess, J. Wahr, J.I. Lunine, J.W. Armstrong, S.W. Asmar, P. Tortora, M. Di Benedetto, P. Racioppa, Can Cassini detect a subsurface ocean in Titan from gravity measurements? *Icarus* **194**, 711–720 (2008)
- E.J. Sauter, S.I. Muyakshin, J.-L. Charlou, M. Schlüter, A. Boetius, K. Jerosch, E. Damm, J.-P. Foucher, M. Klages, Methane discharge from a deep-sea submarine mud volcano into the upper water column by gas hydrate-coated methane bubbles. *Earth Planet. Sci. Lett.* **243**, 354–365 (2006). doi:[10.1016/j.epsl.2006.01.041](https://doi.org/10.1016/j.epsl.2006.01.041)
- P.M. Schenk, W.B. McKinnon, Fault offsets and lateral crustal movement on Europa: evidence for a mobile ice shell. *Icarus* **79**, 75–100 (1989)
- D.J. Sebald, B. D. Van Veen, in *Application of MVDR Beamforming to Reject Turbulence Noise in a Duct*. IEEE International Conference on Acoustics, Speech, and Signal Processing. ICASSP-96. Conference Proceedings, vol. 5 (1996), pp. 2734–2737
- I.C. Shepard, R.F. La Fontaine, Microphone screens for acoustic measurement in turbulent flows. *J. Sound Vib.* **111**(1), 153–165 (1986)
- F. Sohl, M. Choukroun, J. Kargel, J. Kimura, R. Pappalardo, S. Vance, M. Zolotov, Subsurface water oceans on icy satellites: chemical composition and exchange processes. *Space Sci. Rev.* **153**, 485–510 (2010)
- T. Spohn, G. Schubert, Oceans in the icy Galilean satellites of Jupiter? *Icarus* **161**, 456–467 (2003)
- K.M. Stafford, C.G. Fox, D.S. Clark, Long-range acoustic detection and localization of blue whale calls in the northeast Pacific Ocean. *J. Acoust. Soc. Am.* **106**, 3616–3625 (1998)
- M.C. Towner, J.R.C. Garry, R.D. Lorenz, A. Hagermann, B. Hathi, H. Svedhem, B.C. Clark, M.R. Leese, J.C. Zarnecki, Physical properties of the Huygens landing site from the surface science package acoustic properties sensor (API S). *Icarus* **185**, 457–465 (2006)
- B.J. Travis, J. Palguta, G. Schubert, A whole-moon thermal history model of Europa: impact of hydrothermal circulation and salt transport. *Icarus* **218**(2), 1006–1019 (2012)
- R.J. Urick, *Principles of Underwater Sound*, 3rd edn. (McGraw-Hill Book Company, New York, 1983), pp. 120–126
- S. Vance, J. Harnmeijer, J. Kimura, H. Hussmann, B. deMartin, J.M. Brown, *Astrobiology* **7**(6), 987–1005 (2007)
- T. VanHoolst, N. Rambaux, Ö. Karatekin, V. Dehant, A. Rivoldini, The librations, shape, and icy shell of Europa. *Icarus* **195**(1), 386–399 (2008)
- J.S. Wang, M.J. Crocker, Tubular windscreen design for induct fan sound power measurements. *J. Acoust. Soc. Am.* **55**(3), 568–575 (1974)
- P.R. White, Modelling of sound propagation in the ocean, in *Advanced Applications in Acoustics, Noise and Vibration*, eds. by F. Fahy, J. Walker (Spon Press, 2004), pp. 154–180
- P.R. White, T.G. Leighton, D.C. Finfer, C. Powles, O.N. Baumann, Localisation of sperm whales using bottom-mounted sensors. *Appl. Acoust.* **67**, 1074–1090 (2006)
- P.F. Worcester, B.D. Cornuelle, M.A. Dzieciuch, W.H. Munk, B.M. Howe, J.A. Mercer, R.C. Spindel, J.A. Colosi, K. Metzger, T.G. Birdsall, A.B. Baggeroer, A test of basin-scale acoustic thermometry using a large aperture vertical array at 3250-km range in the eastern North Pacific Ocean. *J. Acoust. Soc. Am.* **105**, 3185–3201 (1999)
- J.C. Zarnecki, M.R. Leese, B. Hathi, A.J. Ball, A. Hagermann, M.C. Towner, R.D. Lorenz, J.A.M. McDonnell, S.F. Green, M.R. Patel, T.J. Ringrose, P.D. Rosenberg, K.R. Atkinson, M.D. Paton, M. Banaszekiewicz, B. C. Clark, F. Ferri, M. Fulchignoni, N.A.L. Ghafoor, G. Kargl, H. Svedhem, J. Delderfield, M. Grande, D.J. Parker, P.G. Challenor, J.E. Geake, A soft solid surface on Titan as revealed by the Huygens Surface Science Package. *Nature* **438**, 792–795 (2005)
- C. Zimmer, K.K. Khurana, Subsurface oceans on Europa and Callisto: constraints from Galileo magnetometer observations. *Icarus* **147**, 329–347 (2000)